Journal of Instrumentation

OPEN ACCESS

Efficiency and timing resolution of scintillator tiles read out with silicon photomultipliers

To cite this article: O. Pooth *et al* 2016 *JINST* **11** T01002

View the article online for updates and enhancements.

Related content

- Time resolution below 100 ps for the SciTil detector of PANDA employing SiPM
S E Brunner, L Gruber, J Marton et al.
- Optimization of the light yield properties from scintillator tiles read out directly by silicon photomultipliers
B Bobchenko, M Chadeeva, M Danilov et al.
- Fast SiPM Readout of the PANDA TOF Detector
M. Böhm, A. Lehmann, S. Motz et al.

This content was downloaded from IP address 134.130.184.25 on 18/12/2017 at 15:00

Jinst

PUBLISHED BY IOP PUBLISHING FOR SISSA MEDIALAB

RECEIVED: *October 28, 2015*
ACCEPTED: *December 17, 2015*
PUBLISHED: *January 18, 2016*

TECHNICAL REPORT

Efficiency and timing resolution of scintillator tiles read out with silicon photomultipliers

O. Pooth, S. Weingarten[1] and L. Weinstock

III. Physkalisches Institut B, RWTH Aachen University,
Otto-Blumenthal-Str., 52056 Aachen, Germany

E-mail: weingarten@physik.rwth-aachen.de

ABSTRACT: Silicon photomultipliers (SiPM) are semiconductor photo sensors that have the potential to replace photomultiplier tubes (PMT) in various fields of application. We present detectors consisting of $30 \times 30 \times 0.5\,\mathrm{cm}^3$ fast plastic scintillator tiles read out with SiPMs. The detectors offer great electronic and mechanical advantages over the classical PMT-scintillator combination. SiPMs are very compact devices that run independent of magnetic fields at low voltages and no light guides between the scintillator and the SiPM are necessary in the presented layouts. Three prototypes, two of which with integrated wavelength shifting fibres, have been tested in a proton beam at the COSY accelerator at Forschungszentrum Jülich. The different layouts are compared in terms of most probable pulse height, detection efficiency and noise behaviour as well as timing resolution. The spatial distributions of these properties across the scintillator surface are presented. The best layout can be operated at a mean efficiency of $\overline{\epsilon} = 99.9\,\%$ while sustaining low noise rates in the order of 10 Hz with a timing resolution of less than 3 ns. Both efficiency and timing resolution show good spatial homogeneity.

KEYWORDS: Scintillators, scintillation and light emission processes (solid, gas and liquid scintillators); Photon detectors for UV, visible and IR photons (solid-state) (PIN diodes, APDs, Si-PMTs, G-APDs, CCDs, EBCCDs, EMCCDs etc)

[1]Corresponding author.

Content from this work may be used under the terms of the Creative Commons Attribution 3.0 License. Any further distribution of this work must maintain attribution to the author(s) and the title of the work, journal citation and DOI.

doi:10.1088/1748-0221/11/01/T01002

2016 JINST 11 T01002

Contents

2016 JINST 11 T01002

1 Introduction

Silicon photomultipliers (SiPMs) are of increasing importance, often adopting the role of a semiconductor replacement for photo multiplier tubes (PMTs). They offer excellent light detection properties in a small, affordable device that can be operated in magnetic fields with low bias voltages ($< 100\,\mathrm{V}$) [1]. One classical PMT applications is the combination with various scintillating materials for the detection of ionizing particles. Especially fast plastic scintillators are often used with PMTs for trigger or veto detectors. Naturally, the combination of SiPMs with scintillators is of great interest. A lot of R&D efforts are ongoing in various fields of applications [2, 3] and running systems can already be found in large experiments [4].

In previous studies, we showed promising results with a detector prototype consisting of a $10\times10\times0.5\,\mathrm{cm}^3$ plastic scintillator read out with *Hamamatsu* SiPMs of type S10362-33-100C [5]. In contrast to PMT systems these detectors are designed without complex light guides connecting the scintillator to the SiPM. This leads to compact detectors and the potential for dense multi-module systems with little dead space. With the detector principle tested and optimized, this article investigates whether or not detection quality can be sustained when scaling up to larger scintillator tiles and how homogeneous the detector response is across the surface. Therefore, three prototypes with $30\times30\times0.5\,\mathrm{cm}^3$ scintillators were constructed and tested in a proton-beam at the COSY synchrotron accelerator at Forschungszentrum Jülich [6, 7].

2 Module design

Three different module layouts were tested in the testbeam setup. The simplest design is a plain scintillator directly read out by an SiPM which is mounted at the edge of the scintillator (a large version of the prototype developed in [5]). In addition, two prototypes with integrated wavelength-shifting-fibres (WSF) for better light collection were designed. Figure 1 shows the top-view

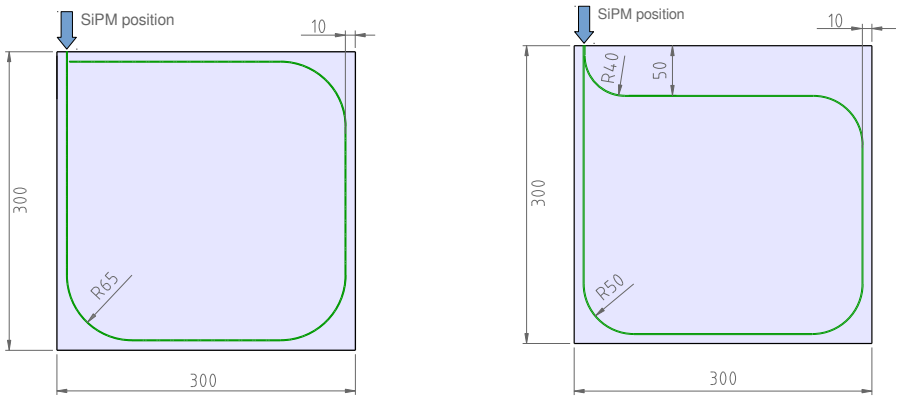

(a) One integrated WSF. **(b)** Two integrated WSF.

Figure 1. Schematics of the $30 \times 30\,\mathrm{cm}^2$ scintillator tiles with one and two integrated WSF, all lengths are given in mm.

blueprints of the fibre layouts. The design of figure 1 (a) uses one WSF arranged in a so-called sigma-groove where one end of the fibre is mirrored inside the scintillator and the other end is optically coupled to an SiPM at the edge of the scintillator. The second layout (figure 1 (b)) uses two WSF, one on the top and one on the bottom surface of the scintillator and a slightly different shape. In this design all four fibre ends are brought back together and coupled to the SiPM to maximize light yield.

All modules are read out by *Hamamatsu* SiPMs of type S10362-33-100C [8]. The active area of the SiPMs is $3 \times 3\,\mathrm{mm}^2$ with a pixel pitch of $100\,\mu$m which leads to a total of 900 pixels. The chosen scintillator is BC-404 by *Saint-Gobain*, which offers a very short decay time of 1.8 ns with the highest light output in the BC-400 series [9]. Since high signals are expected, especially in the fibre modules, the frontend-electronics is modified to provide an additional low-gain output of the SiPM signal. Furthermore, all three modules have been wrapped with *Tyvek* paper (hard-structure type 1082D, $105\,\mathrm{g/m}^3$ [10]) as reflective material, which provides similar reflective properties compared to the also widely-used PTFE *Teflon* tape [11], while being easier to apply to large surfaces.

3 Experimental setup

For the testbeam measurement, the three modules were mounted in layers on an x-y-positioning table and could be moved in the proton-beam. Triggers were generated by the coincidence of two scintillators with PMT readout, one in front of the detectors and one behind. A third scintillator with a 2.5 cm-diameter hole in the middle was used to define the beam-spot on the detectors and veto against scattered particles (figure 2).

The COSY accelerator was configured to deliver protons with an energy of $E = 2.95\,\mathrm{GeV}$ and a momentum of $p = 2.80\,\mathrm{GeV}$ respectively. At this momentum, the energy loss of the protons in the scintillator is minimal, as can be seen in [12, 13]. Therefore, this study represent a worst case scenario for the detection of heavy charged particles, since all other particles will produce at least the same number of photons in the scintillator.

2016 JINST 11 T01002

Figure 2. Picture of the experimental setup in the testbeam facility at Forschungszentrum Jülich.

The peak values of the proton rate were measured in the range of 100 kHz to 120 kHz during extraction cycles of around 200 s. The main data taking was performed with three DRS4 evaluation-boards as digitizers [14], which were configured to a sampling rate of 1 GS/s on the input range of $-0.5\,\mathrm{V} \ldots 0.5\,\mathrm{V}$. For each event and channel the DRS boards can store 1024 samples, which translates to a 1 μs time window. Measurements were taken on a 12×12 array with a step size of 3 cm, resulting in 10×10 trigger areas on the $30 \times 30\,\mathrm{cm}^2$ scintillator and one additional row around the scintillators to check the detector alignment. For each position, 10 000 triggers were recorded.

4 Results and discussion

The first step in analysing the recorded waveforms (e.g. pulse height analysis) is to determine the position of the baseline for each channel. For this purpose waveforms of a measurement-point next to the scintillators were used. Since the protons are not hitting the scintillators these points can be used as noise measurements. The voltage values of all sampled data points (1024 per event) of all triggers are filled into a histogram. The maximum of this distribution represents the most likely voltage at the output channel when no signal is present, which is the definition of the baseline. In this way the baseline is determined for each channel individually.

To protect against false waveform analysis, events that show double or multiple peaks in the trigger PMT channels are removed from the analysis. Also, events with falling edges in the beginning of the signal-waveforms, which can arise from large signals shortly before the trigger generation, are taken out.

2016 JINST 11 T01002

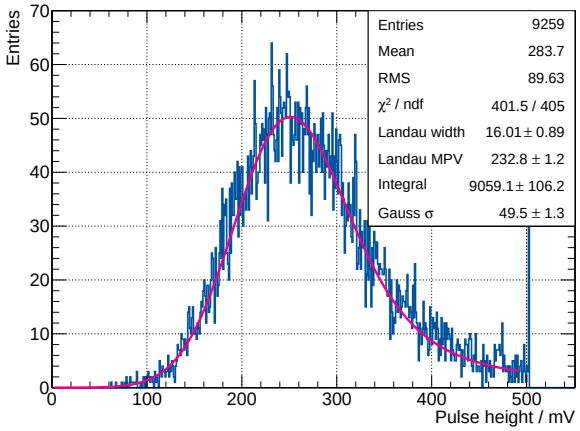

Figure 3. Pulse height distribution with Landau-Gauss fit.

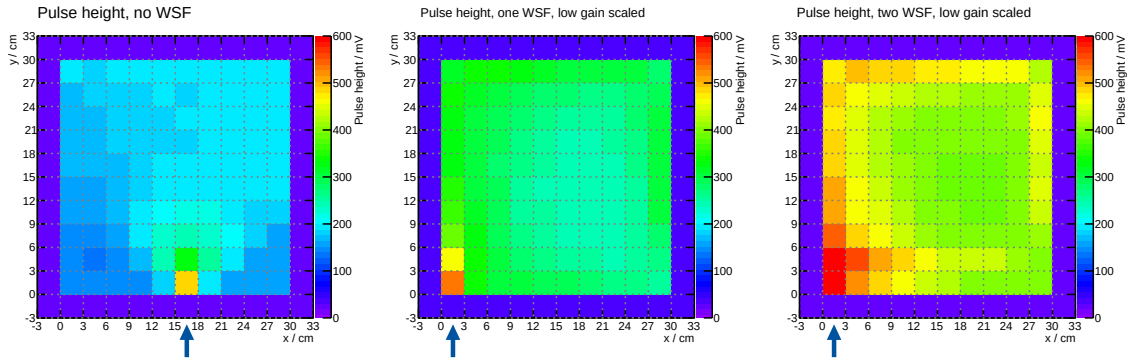

Figure 4. Most probable pulse height distribution on the scintillator surfaces, the arrows indicate the SiPM positions. Left: plain scintillator, middle: one WSF, right: two WSF.

4.1 Pulse height analysis

To analyse the most probable signal height for each trigger position, the pulse heights with respect to the baseline are filled into histograms. A Landau-Gauss convolution is then fitted to the distribution and the maximum of the fitted function represents the most probable pulse height for this measurement point. An example for such a distribution with the fitted function is shown in figure 3. The large overflow bin at 500 mV is due to the limited input range of the DRS4 boards of −0.5 V . . . 0.5 V and not taken into account in the fit. Figure 4 shows the space-resolved distributions of the most probable pulse height (determined by the Landau-Gauss-convolution fit) of the three scintillators. For the modules with integrated fibres the low gain output channels were used and the results are scaled up to the original gain in data for better comparability. The first important information in these plots is the validation of the detector alignment in the proton beam. High signals are clearly visible in the detector region of $0\,\text{cm} < x, y < 30\,\text{cm}$ while the outside measurements show significantly lower noise entries. For the first scintillator, read out directly with an SiPM at $x = 17\,\text{cm}$ (2 cm off-center), signals are in the range of 150 mV – 250 mV. The shape of a light cone is visible, which represents the area from which light can be detected directly by the SiPM. In the bottom corners outside of this cone only reflected light can be detected due to total reflection of direct

2016 JINST 11 T01002

light at the scintillator-SiPM-barrier. Inside this cone the signal height decreases with increasing distance to the SiPM. As expected, the module with an integrated WSF shows significantly larger signals in the region of 250 mV – 400 mV. The benefit of two fibres over one is evident as well with signals between 350 mV and 600 mV in the third module. The fibre layouts in the scintillators can be recognized in the pulse height distribution in form of larger signals near the fibres.

4.2 Detection efficiency and noise rates

The detection efficiency is probably the most important property of a particle detector. It is bound to a detection criterion which is usually defined by a minimal signal height that can easily be realised by a discriminator. But setting the threshold cannot be done universally since there is always a trade-off between gaining a higher efficiency (at lower thresholds) and discriminating against noise pulses (at higher thresholds). Therefore, the efficiency is presented as a function of threshold in combination with the measured SiPM dark count rate for each module (figure 5). The graphics show the rate of noise pulses on the left y-axis and the mean efficiency of the entire scintillator as well as the surface median, the 25% – 75% quantile, and the 10% – 90% quantile on the right y-axis. This shows the homogeneity of the efficiency over the scintillator surface. Once again the detector improvement by integration of fibres is clearly visible. For example the efficiency of the detector with two fibres remains well above 99.5% even when the threshold is configured to suppress all but 1 Hz of noise pulses (at 175 mV). But also the simpler designs can be useful when noise suppression is not as important, for example in setups with an external clock or coincidences of several modules. If noise rates up to O(kHz) are tolerable the one-fibre and no-fibre modules can be used with a mean efficiency of > 99.5% and 95% respectively (at 100 mV).

As an example of the spatial distribution on the scintillator surface, figure 6 shows the detection efficiency of the three modules calculated at a threshold of 150 mV, which corresponds to a noise rate in the order of 10 Hz. In the first plot the light cone structure, which was already present in the pulse height distribution, is once again visible. Outside of this cone, in the bottom corners of the scintillator, the detection efficiency is lowest with about 50%. Inside the cone the efficiency increases to 75% – 100%, depending on the distance to the SiPM. The position of the cone is not symmetrical because the SiPM is not at the center of the scintillator edge. For the detectors with one integrated WSF the efficiency is in the region of 95% – 100%. As expected the module with two fibres shows the best detection efficiency with 99.8% – 100% in the center with only small drops at the edges to 99.6% – 99.7% at worst. Since the lower values are only detected on the very edge of the scintillator, it seems likely, that they are no real inefficiencies rather than particles missing the scintillator, e.g. due to multiple scattering on the vacuum foil of the beam pipe or simply misalignment.

4.3 Signal timing

Beside the detection efficiency and the detector's noise behaviour, signal timing is of great importance. Timing properties are especially interesting when dealing with light collection in large scintillators and light-guiding fibres, which is hard to predict. Before calculating overall timing resolutions for the modules the signal behaviour of each measurement point is presented. A constant fraction discriminator (CFD) is simulated and applied to the recorded data to generate time markers. For this analysis pulses with a minimum signal height of 100 mV and a CFD setting of 50% are used. The signal of the front trigger PMT is used as reference and the distributions of

2016 JINST 11 T01002

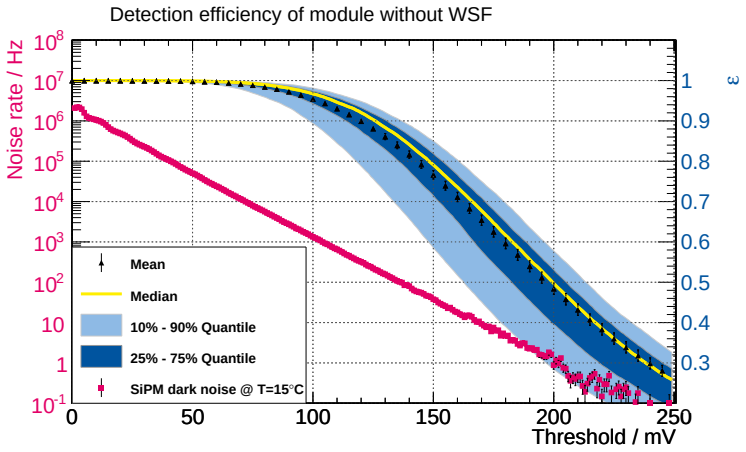

(a) No integrated WSF.

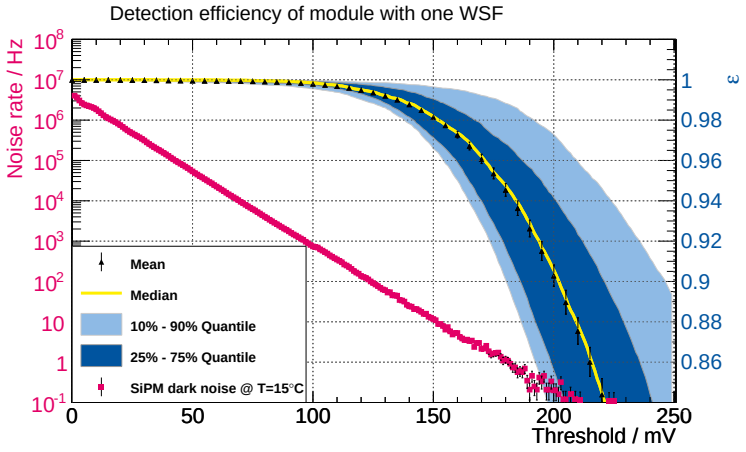

(b) One integrated WSF.

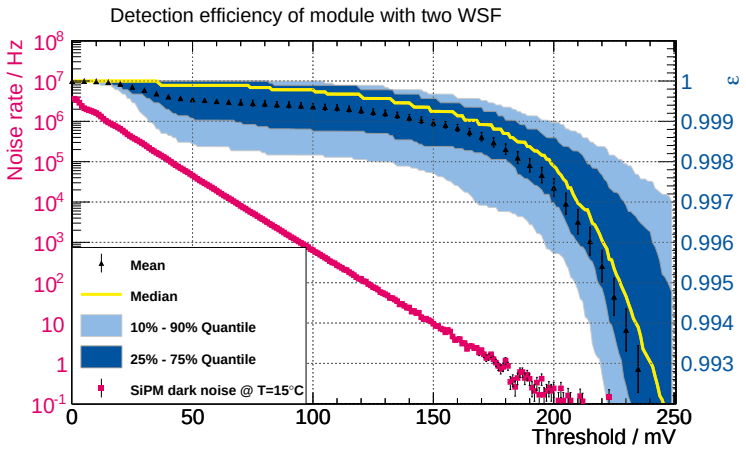

(c) Two integrated WSF.

Figure 5. SiPM dark noise (left y-axis) and detection efficiency (right y-axis) as function of discriminator threshold for all modules (consider the different scales on the efficiency axes).

2016 JINST 11 T01002

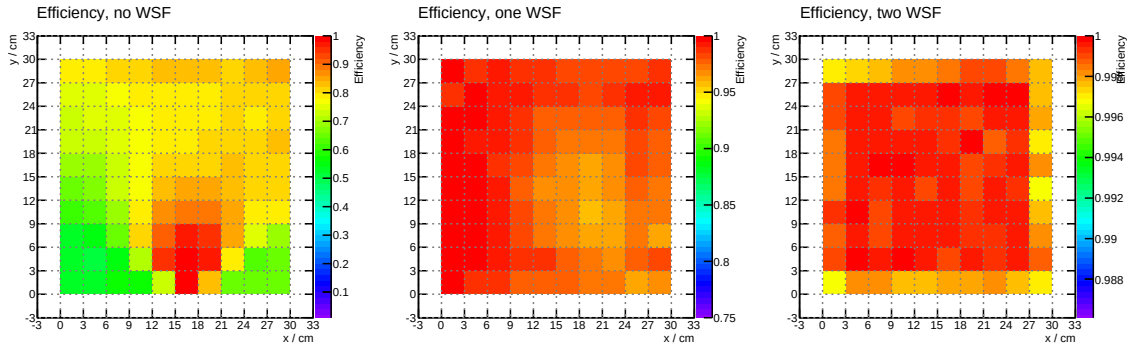

Figure 6. Detection efficiency at a simulated threshold of 150 mV (consider the different z-axis scales).

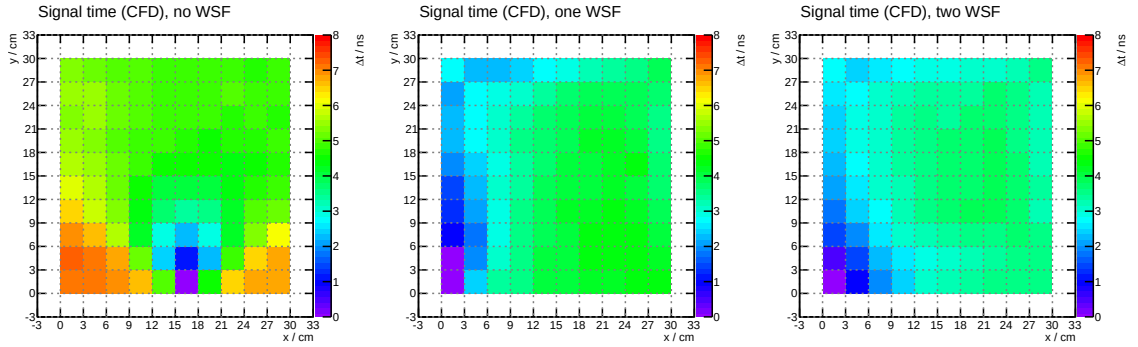

Figure 7. Mean signal time of pulses > 100 mV with CFD set to 50%.

time differences Δt to this reference are calculated. These distributions are fitted with Gaussians, where the mean provides information about the arrival time of the signal with respect to the chosen reference. The spatial distribution over the detector surface is shown in figure 7. The lowest value of each module is set to 0 ns and all other values are given relative to this point.

As expected, in all modules the signal is fastest when hitting the scintillator right in front of the SiPM. Furthermore, the arrival time distributions once again reflect the distinct features of the modules, namely the light cone at the direct readout and the WSF in the other modules. For all three modules, for the major part of the surface it takes around 4 ns longer to generate the signal compared to hits directly in front of the SiPM. In the first detector, hits outside the light cone lead to longer light collection times due to the fact, that the photons cannot be detected directly. The fibre detectors on the other hand show faster signals when hit near the integrated fibres.

The width σ of the fitted Gaussians is given by the combined timing resolution of the detector and the trigger PMT:

$$\sigma_t \equiv \sigma(t_{\mathrm{Det}} - t_{\mathrm{PMT}}) = \sqrt{\sigma^2_{t_{\mathrm{Det}}} + \sigma^2_{t_{\mathrm{PMT}}} + (400\,\mathrm{ps})^2}$$

in which the 400 ps account for the timing resolution between two different DRS4 boards that are triggered in a daisy chained setup [14]. With help of the second trigger PMT, three time differences

2016 JINST 11 T01002

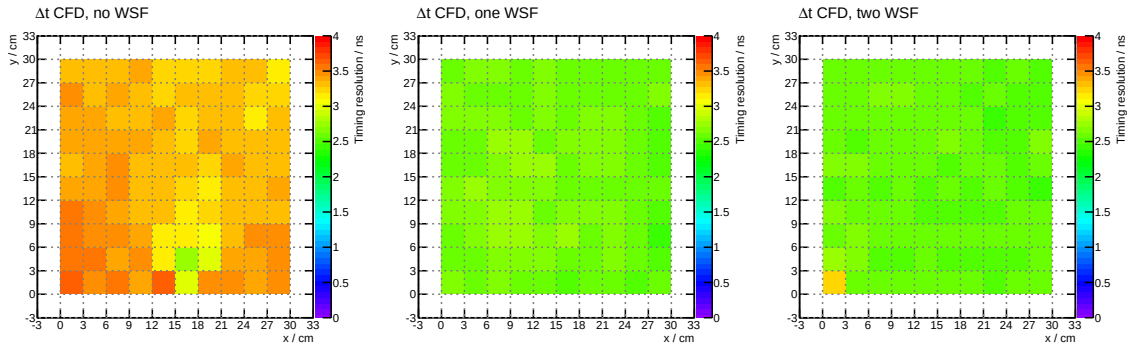

Figure 8. Timing resolution of pulses > 100 mV with CFD set to 50%.

can be calculated. The widths of these three distributions are given by:

$$\sigma_1 \equiv \sigma(t_{\mathrm{PMT1}} - t_{\mathrm{PMT2}}) = \sqrt{\sigma^2_{t_{\mathrm{PMT1}}} + \sigma^2_{t_{\mathrm{PMT2}}}}$$

$$\sigma_2 \equiv \sigma(t_{\mathrm{Det}} - t_{\mathrm{PMT1}}) = \sqrt{\sigma^2_{t_{\mathrm{Det}}} + \sigma^2_{t_{\mathrm{PMT1}}} + (400\,\mathrm{ps})^2}$$

$$\sigma_3 \equiv \sigma(t_{\mathrm{Det}} - t_{\mathrm{PMT2}}) = \sqrt{\sigma^2_{t_{\mathrm{Det}}} + \sigma^2_{t_{\mathrm{PMT2}}} + (400\,\mathrm{ps})^2}$$

With these σ_i, which are measured, $\sigma_{t_{\mathrm{Det}}}$ can be expressed as:

$$\sigma_{t_{\mathrm{Det}}} = \sqrt{\frac{1}{2} \cdot \left(\sigma_2^2 + \sigma_3^2 - \sigma_1^2 - 2 \cdot (400\,\mathrm{ps})^2\right)}$$

In this way the timing resolution of the tested detectors can be calculated independently of the trigger PMT's timing resolution. This is done for each point and shown in figure 8. The timing resolution of the single measurements is distributed more homogeneously than the arrival times and values are in order of 3 ns – 4 ns for the first module and 2 ns – 2.5 ns for the fibre modules.

In order to calculate an overall timing resolution for each detector independent of the hit position, the described Δt distributions have to be combined. Therefore, the recorded distributions are weighted with the inverse number of entries for each measurement point and added. The width of this sum distribution then yields the timing resolution of the given module for an unknown particle hit location. Since this sum of Gaussians with different mean values is no longer gaussian, the RMS is used as measure of the width. The timing resolution is again calculated with help of the PMT signals as described above. This gives $\Delta t = 4.10$ ns for the module without WSF, $\Delta t = 3.20$ ns with one integrated WSF, and $\Delta t = 2.85$ ns for the prototype with two fibres.

5 Conclusion

Testbeam results of fast scintillation detectors for ionizing particles with a large detection area of $30 \times 30\,\mathrm{cm}^2$ and SiPM readout have been presented. The analysis shows the different capabilities of simple and more sophisticated designs and the distinct features of each layout are clearly visible in recorded data. The discussion reveals the potential of these scintillator-SiPM combinations. They can compete with classical PMT solutions in terms of detection efficiency and noise behaviour

2016 JINST 11 T01002

while allowing very compact detector designs. Furthermore, timing resolutions down to 2.85 ns have been measured.

A possible improvement to these detectors is to replace the S10362-33-series SiPMs with newer models, where noise effects have been significantly reduced [1]. SiPMs of the *Hamamatsu* series S13360 are currently being tested. The improved signal to noise ratio will allow simple designs to compete with the presented two-fibre module and therefore allow for cheaper detector construction. Furthermore, wavelength shifting fibres with larger diameters as well as fibres with square cross section are of interest to improve light yield.

References

[1] Hamamatsu, *MPPC and MPPC module for precision measurement*, brochure, (2015).

[2] LHCb SciFi Tracker group collaboration, Z. Xu et al., *Silicon photomultipliers for the LHCb upgrade scintillating fibre tracker*, PoS(TIPP2014)071.

[3] Y. Lu et al., *Development of a SiPM-based PET imaging system for small animals*, *Nucl. Instrum. Meth.* **A 743** (2014) 30.

[4] CMS collaboration, B. Lutz, *Upgrade of the CMS hadron outer calorimeter with SiPM sensors*, *J. Phys. Conf. Ser.* **404** (2012) 012018.

[5] O. Pooth et al., *Scintillator tiles read out with silicon photomultipliers*, 2015 *JINST* **10** T10007.

[6] R. Maier, *Cooler synchrotron COSY — performance and perspectives*, *Nucl. Instrum. Meth.* **A 390** (1997) 1.

[7] C. Weidemann et al., *Toward polarized antiprotons: machine development for spin-filtering experiments*, *Phys. Rev. ST Accel. Beams* **18** (2015) 020101 [arXiv:1407.6724].

[8] Hamamatsu, *S*10362-33-*series*, data sheet, (2009).

[9] Saint Gobain, *Plastic scintillators*, data sheet, (2014).

[10] DuPont, *Typical properties of Tyvek style* 10, data sheet, (2008).

[11] S.P. Stoll, *An investigation of the reflective properties of Tyvek papers and Tetratex PTFE film*, PHENIX note #245, (1996).

[12] Particle Data Group collaboration, K.A. Olive et al., *Review of particle physics*, *Chin. Phys.* **C 38** (2014) 090001.

[13] Particle Data Group collaboration, 32. *Passage of particles through matter*, figure 32.2, (2014).

[14] S. Ritt, *DRS*4 *evaluation board — user's manual*, board revision 5, (2014).

2016 JINST 11 T01002